Interfacial Dzyaloshinskii-Moriya interaction and dampinglike spin-orbit torque in $[Co/Gd/Pt]_N$ magnetic multilayers

Tomoe Nishimura,[1,*] Dae-Yun Kim,[2,3,*] Duck-Ho Kim,[1,3,†] Yune-Seok Nam,[2] Yong-Keun Park,[2,3] Nam-Hui Kim,[4] Yoichi Shiota,[1] Chun-Yeol You,[4] Byoung-Chul Min,[3] Sug-Bong Choe,[2,‡] and Teruo Ono[1,5,§]

[1]*Institute for Chemical Research, Kyoto University, Uji, Kyoto 611-0011, Japan*

[2]*Department of Physics and Institute of Applied Physics, Seoul National University, Seoul, 08826, Republic of Korea*

[3]*Center for Spintronics, Korea Institute of Science and Technology (KIST), Seoul 02792, Republic of Korea*

[4]*Department of Emerging Materials Science, Daegu Gyeongbuk Institute of Science and Technology (DGIST), Daegu 42988, Republic of Korea*

[5]*Center for Spintronics Research Network (CSRN), Graduate School of Engineering Science, Osaka University, Toyonaka, Osaka 560–8531, Japan*

(Received 24 November 2019; revised 17 February 2021; accepted 18 February 2021; published 4 March 2021)

Recently, magnetic multilayer systems have received again a great attention owing to their suitability for the generation of magnetic chiral spin structure. In this study, we experimentally investigated the interfacial Dzyaloshisnkii-Moriaya interaction (DMI) and the spin-Hall angle (SHA) of magnetic Co/Gd/Pt multilayers with respect to the repetition number N of the multilayers. The DMI and SHA are important variables that govern the stability and mobility of a homochiral spin structure, respectively. The experimental results show that the ratio between the DMI and the dipole energy from the domain wall gradually decreases as N increases, which is expected to be hard to achieve homochiral spin structure for larger N and the values of SHA remain constant irrespective of N. The observed SHA invariance indicates that the Pt layers in repetition have a negligible effect on the SHA.

DOI: 10.1103/PhysRevB.103.104409

I. INTRODUCTION

The inversion symmetry breaking with strong spin-orbit coupling (SOC) at the interfaces between a heavy-metal (HM) and a ferromagnetic-metal (FM) bilayer results in an antisymmetric exchange interaction. This interaction is known as the interfacial Dzyaloshinskii-Moriya interaction (DMI) [1,2]. The DMI plays a key role in the formation of chiral spin textures [3–18] such as magnetic skyrmions and chiral Néel domain walls (DWs). A strong SOC and large inversion asymmetry are the key factors for engineering the DMI strength in HM/FM interfaces. Recently, theoretical and experimental studies for manipulating the interfacial DMI have been reported; different HM materials in HM/FM/HM (or HM/FM/Oxide) trilayers were chosen in these studies [19–21]. Several researchers have experimentally demonstrated the correlation of interfacial DMI with the anisotropies of orbital magnetic moment and magnetic dipole moment [22] as well as the work function difference at interfaces [19]. These experimental findings provide useful guidelines for engineering interfacial DMI, using suitable interface materials. Therefore, numerous studies have been devoted to investigating HM/FM/HM trilayers (or HM/FM bilayers) with various HM materials.

When in-plane charge current passes through the HM layers in HM/FM/HM trilayered films, a nonzero, out-of-plane spin current is induced into the adjacent FM layer owing to strong SOCs. These spin currents can exert spin torques—known as spin-orbit torques (SOTs) [23–28]—on the magnetic moment in the FM layer. Thus, SOTs provide an efficient way to manipulate magnetization, including magnetization switching [24,25]. Even though the principle has been verified for understanding of its physics, the appropriate materials and layered structures still need to be investigated for its application. A number of studies have attempted to identify suitable materials by focusing on materials exhibiting strong SOCs and with different HM materials [19,20] or by replacing HM materials with topological insulators [29]. Antiferromagnetic materials or ferrimagnetic (FiM) materials have been employed because fast magnetization manipulation is expected owing to the antiferromagnetically coupled magnetic moments in these materials [30–32]. Similar to the studies on DMI, a majority of the studies on SOT have also focused on investigating materials possessing bilayer or trilayer structures.

Superlattices and multilayers have received a great attention once again owing to their suitability for the generation of magnetic skyrmions [33]. Moreover, they exhibit high signal-to-noise ratios of magnetic signals and high thermal stabilities of magnetic states [34]. Meanwhile because it is known that interfacial phenomena such as DMI and SOT can be manipulated by adjusting the number of interfaces, it is possible to engineer the DMI and SOT strengths by regulating the repetition number of the superlattices and multilayers [33]. There

*These authors contributed equally to this work.
†uzes@kist.re.kr
‡sugbong@snu.ac.kr
§ono@scl.kyoto-u.ac.jp

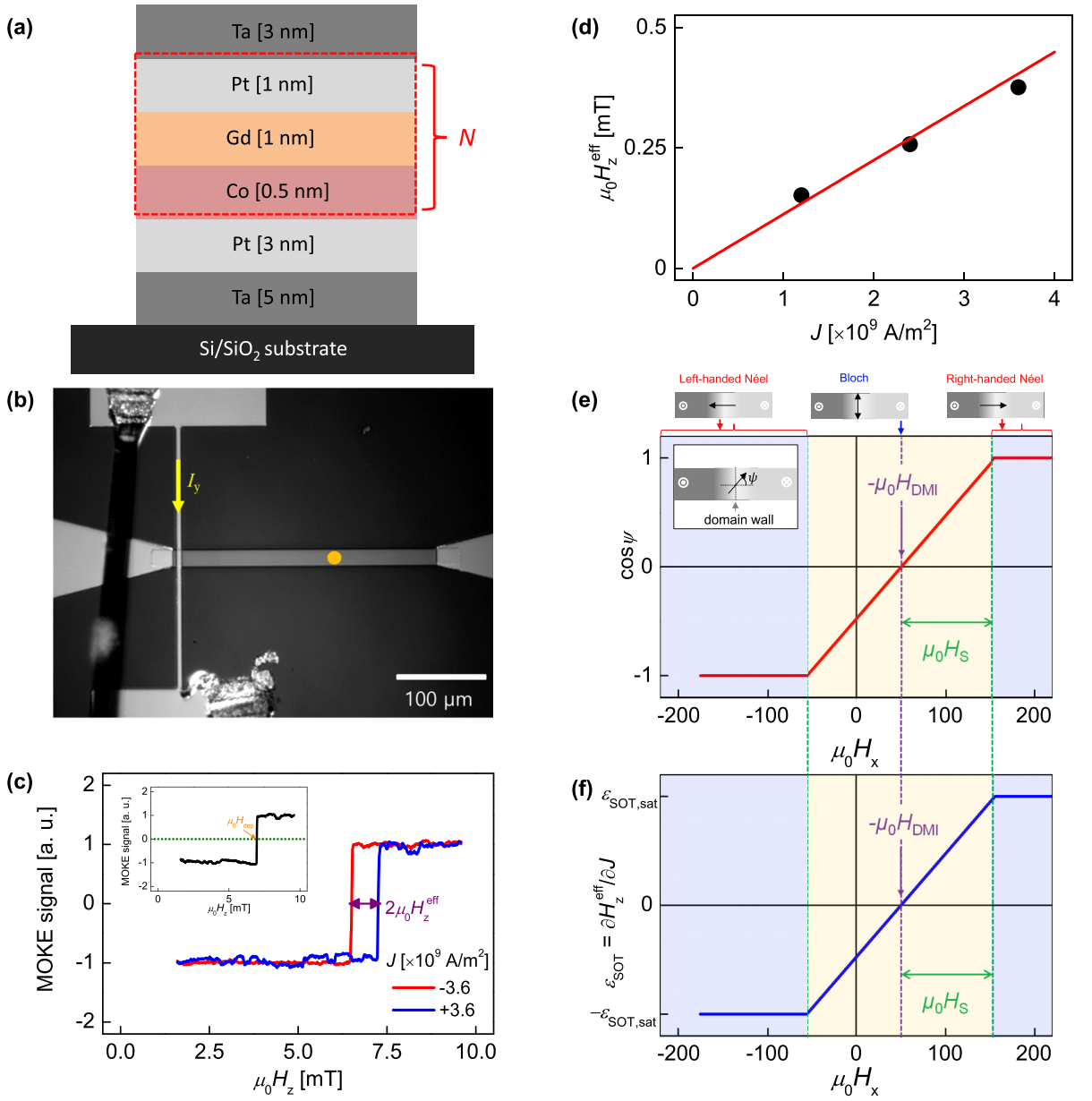

FIG. 1. (a) Schematic diagram of sample structure. (b) Captured charge-coupled device (CCD) image of micropatterned device. Yellow arrow indicates current flow along the Au wire for DW writing. Orange dot presents laser-beam spot for the MOKE measurements. The inset presents up and down magnetic domains and a magnetic domain wall, where ψ is the azimuthal angle of the DW center magnetization. (c) Plots of MOKE signal as a function of $\mu_0 H_z$ with positive (blue), negative (red) current bias, and without current bias (inset). The purple arrow presents effective field induced by the current bias. (d) Plot of $\mu_0 H_z^{\rm eff}$ as a function of J. The red dotted line indicates the best linear fitting. (e) Schematics of the DW types and $\mu_0 H_x$ dependent of the azimuthal angle ψ of the DW center magnetization. (f) Damping-like SOT efficiency $\varepsilon_{\rm SOT} = \varepsilon_{\rm SOT,sat} \cos\psi(\mu_0 H_x)$ under $\mu_0 H_x$, where $\varepsilon_{\rm SOT,sat}$ is the SOT efficiency of the Néel-type DWs.

have been many experimental results about the DMI and SOT in bilayer- and trilayer-layered structures, however, systematic studies on the DMI and SOT in multilayered structures have not been explored yet.

In this study, we systematically investigated the strength of the interfacial DMI from the FiM/HM bilayer to the $[\mathrm{FiM/HM}]_N$ multilayers by varying the repetition number N. Our experimental findings reveal that the strength of the DMI-induced effective field decreases with N. We also investigated the dampinglike SOT efficiency as a function of N, and the spin-Hall angle (SHA) is found to remain approximately constant with respect to N.

II. SAMPLE PREPARATION AND EXPERIMENTAL SETUP

In this study, Ta (5 nm)/Pt(3 nm)/$[$Co(0.5 nm)/Gd(1 nm)/Pt(1 nm)$]_N$/Ta(3 nm) magnetic multilayers were fabricated on an $\mathrm{Si/SiO_2}$ substrate by using DC magnetron sputtering, where N represents the repetition number, as schematically shown in Fig. 1(a). N was varied from 1 to 5. Please note that

the upper limit of N was determined by the DW roughness; as increasing N, the perpendicular magnetic anisotropy (PMA) would be relatively weaker than the magnetostatic energy, and thus, the DW becomes much rougher so that the uniform DW motion cannot be observed anymore. Moreover, the homogeneity of the DW normal, which is an important factor in the analysis of the SOT, is not guaranteed for $N > 6$. According to our previous report [35], we indeed observed that the magnetic reversal phase has a gradual transition from the uniform DW motion to the dendritic domain expansion. Meanwhile, the films include a nonmagnetic heavy metal layer (Pt) as a source of the spin current for the effects of spin-orbit torque [23–28]. It must be noted that inevitable intermixing exists between ferrimagnetic layers and heavy metal layers because the film was fabricated by the sputtering technique. However, the transmission electron microscopy image, which was shown in our previous report [35], revealed that the interface between the layers is well defined, showing a low degree of intermixing.

Figure 1(b) depicts the optical microscope image of the device of 20-μm width and 500-μm length; the device is optimized for observing current-induced DW motion. By inducing a current pulse through a writing line vertically crossing a magnetic wire, a reversed domain can be nucleated under the writing line by the highly localized Oersted's field [15,16]. As a result, the initial DW can be repeatedly and intentionally created.

To obtain the SOT and DMI, we investigate the depinning field of the DWs as a function of the in-plane magnetic field $\mu_0 H_x$. The measurement procedure proposed in previous studies was applied [16,36–39]. Initially, we applied a sufficiently strong perpendicular magnetic field (+80 mT) to saturate the magnetization. To nucleate the reversed domain, a current pulse was induced in the writing line [indicated by the yellow arrow in Fig. 1(b)], thereby creating a single reversed domain in the magnetic wire. Subsequently, under the application of a fixed current bias, we swept the perpendicular magnetic field $\mu_0 H_z$ until the DW reached the position of the laser spot for the detection of the magneto-optical Kerr effect (MOKE) signal [the laser spot as indicated by the orange circular dot shown in Fig. 1(b)]. The inset of Fig. 1(c) presents the normalized MOKE signal as a function of $\mu_0 H_z$ under $J = 0$ A/m^2 and $\mu_0 H_x = -160$ mT. A sign inversion in the MOKE signal indicates the depinning field $\mu_0 H_{\rm dep}$ [as indicated by the orange arrow in the inset of Fig. 1(c)]. Figure 1(c) depicts the normalized MOKE signals as a function of $\mu_0 H_z$ for different bias currents of $J = \pm 3.6 \times 10^9$ A/m^2 under a constant $\mu_0 H_x = -160$ mT. $\mu_0 H_{\rm dep}$ is shifted under the positive and negative bias currents due to the effective magnetic field $\mu_0 H_z^{\rm eff}$ due to the SOT [16,36–39] [as shown in Fig. 1(c)]. Here, we define $\mu_0 H_z^{\rm eff} = [\mu_0 H_{\rm dep}(+J) - \mu_0 H_{\rm dep}(-J)]/2$. By repeating this procedure under different bias currents, we measured $\mu_0 H_z^{\rm eff}$ as a function of J for each $\mu_0 H_x$. Figure 1(d) shows $\mu_0 H_z^{\rm eff}$ as a function of the current density J for $\mu_0 H_x = -40$ mT. The slope shown in Fig. 1(d) represents the SOT efficiency $\varepsilon_{\rm SOT} = \partial \mu_0 H_z^{\rm eff}/\partial J$. Note that $\varepsilon_{\rm SOT} = \partial \mu_0 H_z^{\rm eff}/\partial J$ represents the efficiency of current density J in generating an effective magnetic field $\mu_0 H_z^{\rm eff}$ in the DW. $\varepsilon_{\rm SOT}$ depends on $\mu_0 H_x$ because of the type of the DW [16,36–39].

The inset of Fig. 1(e) shows the schematics of the DW, which shows $\mu_0 H_x$ dependent of the azimuthal angle ψ of the DW center magnetization. The DW types can be defined by ψ, where the Bloch-type DW corresponds to $\psi = \pm\pi/2$, the left-handed Néel-type DW corresponds to $\psi = \pi$, and the right-handed Néel-type DW corresponds to 0 [see the top of Fig. 1(e)]. From the counterbalance between the DMI, the DW anisotropy energy (i.e., dipole energy from the DW magnetization), and the Zeeman energy from the external magnetic field $\mu_0 H_x$, the equilibrium equations as a function of $\mu_0 H_x$ are given by [11–13]

$$\cos\psi(\mu_0 H_x) = \begin{cases} \frac{\mu_0 H_x + \mu_0 H_{\rm DMI}}{\mu_0 H_{\rm S}} & \text{for } |\mu_0 H_x + \mu_0 H_{\rm DMI}| < \mu_0 H_{\rm S} \\ \pm 1 & \text{otherwise} \end{cases}, \quad (1)$$

for the equilibrium angle ψ. Here, DW anisotropy field $\mu_0 H_{\rm S}$ is $4K_{\rm D}/\pi M_{\rm S}$ that is required to achieve the Néel-type DW from Bloch-type DW where $K_{\rm D}$ is the DW anisotropy energy density [see the green arrow in the Fig. 1(e)]. The Eq. (1) implies that $\cos\psi = 0$ is achieved only when $\mu_0 H_x$ compensates the DMI-induced effective magnetic field $\mu_0 H_{\rm DMI}$ (i.e. $H_x = -H_{\rm DMI}$). Because the amplitude of the dampinglike SOT on the DW depends on the relative direction between the magnetization in the DW center and the spin current induced by heavy-metal layer [16,36–39], the dampinglike SOT efficiency $\varepsilon_{\rm SOT}$ under $\mu_0 H_x$ is given by $\varepsilon_{\rm SOT} = \varepsilon_{\rm SOT,sat} \cos\psi(\mu_0 H_x)$ [see the green arrow in the Fig. 1(f)]. Please note that $\varepsilon_{\rm SOT,sat}$ is the SOT efficiency of the Néel-type DWs.

III. RESULTS AND DISCUSSIONS

As shown in Fig. 2, $\varepsilon_{\rm SOT}$ was measured by varying the in-plane magnetic field $\mu_0 H_x$ for the present sample series. $\varepsilon_{\rm SOT}$ exhibits a typical antisymmetric behavior with respect to $\mu_0 H_x$. The DMI was quantified from the $\varepsilon_{\rm SOT}$ curves. As mentioned before, $\varepsilon_{\rm SOT}$ depends on the type of DW. Its magnitude exhibits a maximum for the Néel-type DW ($\varepsilon_{\rm SOT} = \pm\varepsilon_{\rm SOT,sat}$) and a minimum for the Bloch-type DW ($\varepsilon_{\rm SOT} = 0$) [16,36–39]. Therefore, the x intercept (i.e., $\varepsilon_{\rm SOT} = 0$) of the curves shown in Fig. 2 corresponds to the Bloch type DW. Since the Bloch-type DW is achieved only when $\mu_0 H_x$ completely compensates the DMI-induced effective magnetic field $\mu_0 H_{\rm DMI}$ [11,13,16], finding the x intercept of the $\varepsilon_{\rm SOT}$ curve provides the direct determination of $\mu_0 H_{\rm DMI}$. The determined $\mu_0 H_{\rm DMI}$ values were plotted as a function of N, as shown in Fig. 3(a). The magnitude of $\mu_0 H_{\rm DMI}$ decreases with N; a decrease of up to 20% was observed. The DW barely maintains the Néel-type DW structure when $N = 5$, but it is expected that the DW will not be able to maintain the Néel-type DW structure when $N > 5$.

The most important role of the DMI in spintronics applications is to stabilize the homochiral Néel-type DWs or topological skyrmions. The "intrinsic" chirality of DWs is determined by competition of the DMI and the dipole-dipole interaction, which is also described in Sec. II. The dipole-dipole interaction prefers the DW chirality to be the Bloch type and thus, it gives rise to an effective in-plane magnetic field $H_{\rm S}$, which is conventionally called DW anisotropy field.

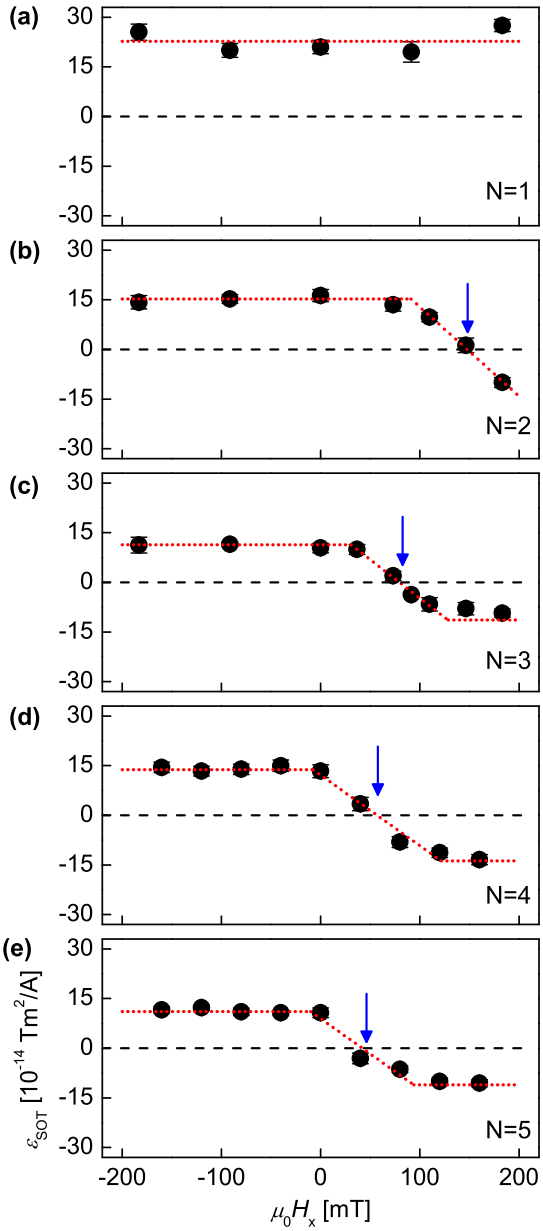

FIG. 2. Plots of ε_{SOT} as a function of $\mu_0 H_x$ for the present sample series. Red dotted lines guide the antisymmetric behavior of ε_{SOT}. Blue arrows indicate $\mu_0 H_x$, which completely compensates the DMI-induced effective field.

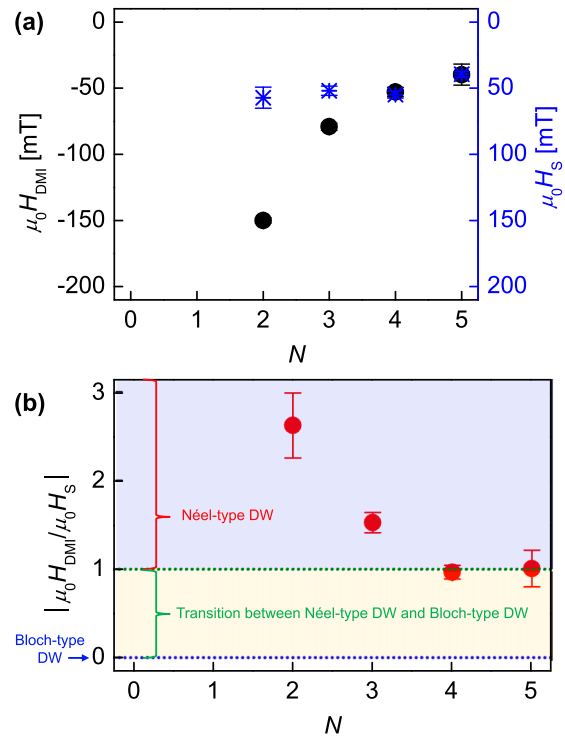

FIG. 3. (a) Plot of $\mu_0 H_{DMI}$ and $\mu_0 H_S$ as a function of N. (b) $|H_{DMI}/H_S|$ as a function of N.

Introducing the concept of H_S is useful because it enables direct comparison to H_{DMI}. Simply, one can categorize the DW type of the initial state by using the ratio between H_{DMI} and H_S; a Néel-type DW for $|H_{DMI}/H_S| \geqslant 1$, a transition between the Néel-type DW and Bloch-type DW for $0 < |H_{DMI}/H_S| < 1$, and a Bloch-type DW for $|H_{DMI}/H_S| = 0$. For example, for the generation of homochiral Néel-type DWs or topological skyrmions with $Q = \pm 1$, H_{DMI} and H_S should meet the condition of $|H_{DMI}/H_S| \geqslant 1$. As shown in Fig. 3(a), H_{DMI} is observed to decrease, while H_S is observed to be almost constant by increasing N. Therefore $|H_{DMI}/H_S|$ gradually decreases as N increases as shown in Fig. 3(b). In the figure, $|H_{DMI}/H_S|$ is barely larger than the unity, which implies that the homochiral Néel-type DWs can be achieved up to $N = 5$. However, considering the decreasing tendency of H_{DMI}/H_S with N, it is expected to be hard to achieve chiral spin structure for larger N.

Subsequently, the SOT was quantified from the ε_{SOT} curves. To consistently compare ε_{SOT} for different N, the maximum ε_{SOT} values that corresponds to the saturation value $\varepsilon_{SOT,sat}$, were adopted for the comparison, as shown in Fig. 4(a). The maximum value of $\varepsilon_{SOT,sat}$ monotonically decreases with N; a decrease of up to 50% was observed, which is similar to the behavior of the maximum $\mu_0 H_{DMI}$ shown in Fig. 3(a).

To understand the decreasing tendency of $\varepsilon_{SOT,sat}$, we investigated the spin-Hall angle. The SHA θ_{SH} can be extracted from $\varepsilon_{SOT,sat}$ by using the following relation:

$$\theta_{SH} = (2eM_S t_{mag}/\hbar)\varepsilon_{SOT,sat}, \quad (2)$$

where M_S is the saturation magnetization, and t_{mag} is the total thickness of the magnetic layer. To extract the values of θ_{SH}, the total Co/Gd layer thickness was treated as t_{mag}, and M_S was experimentally measured using a superconducting quantum interference device magnetometer at 300 K, as shown in Fig. 4(b).

The θ_{SH} calculated using Eq. (2) was plotted as a function of N, as shown in Fig. 4(c). θ_{SH} is found to remain constant with N, which is a clearly different behavior from that of $\varepsilon_{SOT,sat}$. The blue dot line in Fig. 4(c) corresponds to $\theta_{SH} = 0.13$. The constant behavior of θ_{SH} can be attributed to the negligible contribution of HM layers (i.e., Pt layers) inside the repeated stacks to the net spin current. Under the application

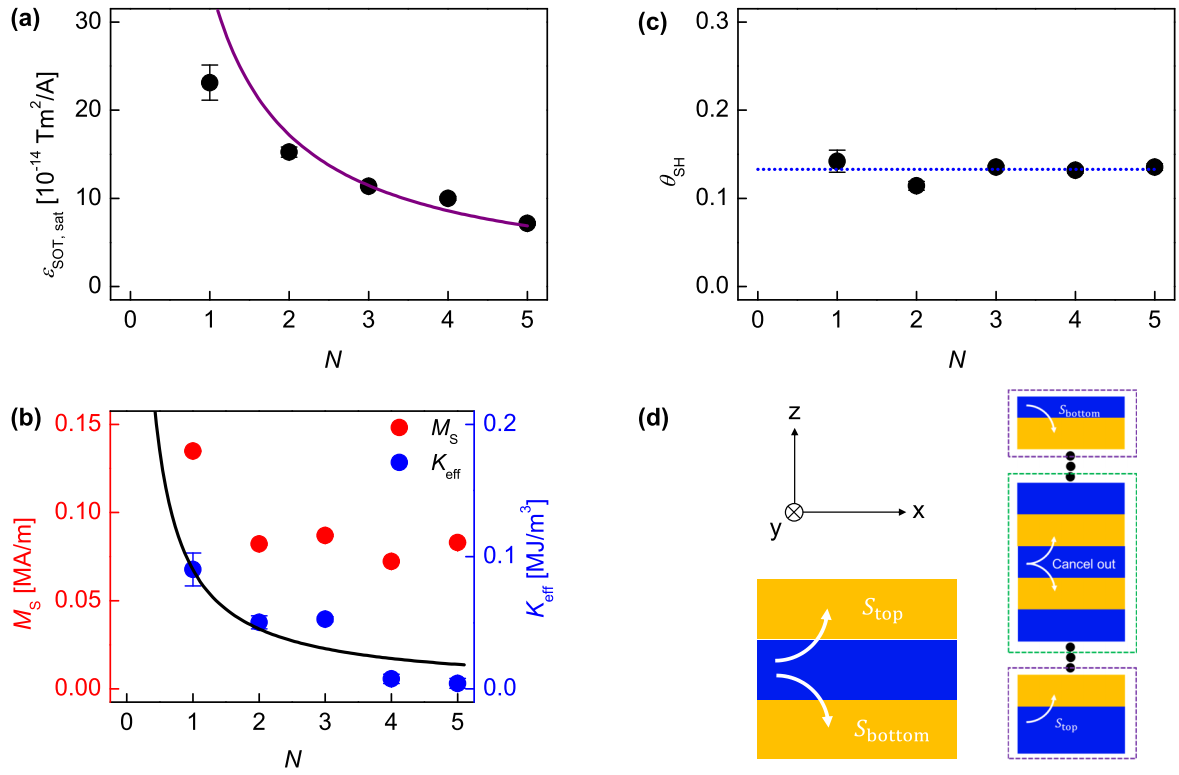

FIG. 4. Plots of (a) $\varepsilon_{SOT,\,sat}$ as a function of N. Purple curve in Fig. 3(a) indicates the inverse proportionality between $\varepsilon_{SOT,sat}$ and N. (b) Plots of M_S (red) and K_{eff} (blue) as a function of N. The black solid line in Fig. 4(b) represents the best fitting based on Eq. (3). (c) Plot of θ_{SH} as a function of N. The blue dotted line represents constant behavior of θ_{SH}. (d) Illustration describing the action of the spin-Hall effect in the present multilayer system. The blue and orange boxes correspond to the heavy-metal and ferrimagnet layer, respectively. The purple and green dashed box denotes top- and bottom-most stack and repetition stack, respectively.

of an in-plane current along the x direction, the spin-Hall-effect-induced spin currents S_{top} and S_{bottom} diffuses from the HM layer (blue box) to the adjacent upper and lower ferrimagnetic Co/Gd layers (orange boxes), respectively, as shown in the left side of Fig. 4(d). It is well known that S_{top} and S_{bottom} has identical magnitudes but opposite polarities (i.e., $S_{top} = -S_{bottom}$) [36]. Therefore, the HM layers inside repeated stack do not contribute to the net spin current of the multilayers, as shown in the right side of Fig. 4(d); their contributions to the net spin current is zero (i.e., $S_{top} + S_{bottom} = 0$). In contrast to these HM layers inside the repeated stack, the bottom-most HM layer, Ta(5-nm)/Pt(3-nm), and the top-most heavy-metal layer, Ta(3-nm), can contribute to the net spin current. It is because the bottom- and top-most HM layers have only one adjacent magnetic layer; one of the spin currents (S_{top} or S_{bottom}) contributes to the net spin current. Furthermore, $\varepsilon_{SOT,sat}$ should be inversely proportional to N according to the present framework; the total magnetic moments increase with proportional to N, while the total spin current remains constant. This inverse-proportionality is clearly observed in Fig. 4(a) by the purple curve, which represents the best fit based on the inverse function.

Lastly, we discuss the decreasing tendency of the perpendicular magnetic anisotropy energy K_{eff} with respect to N. K_{eff} can be considered to be composed of two different magnetic anisotropy energies, $K_{N=1}$ for $[Co/Gd/Pt]_{N=1}$ and K_{N-1} for $[Co/Gd/Pt]_{N=1}$. Then, the total anisotropy energy K_{eff} can be written as

$$K_{eff} = \frac{K_{N=1} + (N-1)K_{N-1}}{N}. \tag{3}$$

The black solid line in Fig. 4(b) represents the best fitting based on Eq. (3). The best fitting parameters are found to be $K_{N=1} = (9 \pm 1) \times 10^4\,J/m^3$ and $K_{N-1} = (7 \pm 1) \times 10^2\,J/m^3$. $K_{N=1} \gg K_{N-1}$ implies that the PMA mainly originates from the $[Co/Gd/Pt]_{N=1}$ (i.e., the interface between the 3 nm-thick buffer Pt layer and the adjacent Co layer). The negligibly small PMA for $[Co/Gd/Pt]_{N=1}$ can be attributed to the thinner Pt layers in the repetition stack [40,41] and/or to the severe interfacial mixing between the Gd and the Pt layers [42].

IV. CONCLUSION

In summary, we investigated the SOT and the DMI in ferrimagnetic multilayers $[Co(0.5\,nm)/Gd(1\,nm)/Pt(1\,nm)]_N$ by varying repetition number of the multiplayers. The experimental results revealed that the SHA remains approximately constant with respect to the varying repetition number. This invariance of the SHA can be attributed to the negligible contribution of the heavy metal layers inside the repeated stack. The ratio between DMI and dipole energy of the DW's magnetization decreases with respect to the repetition number, which means that it's hard to achieve homochiral spin

structure for larger repetition number. Our finding shows that the SOT efficiency and the DMI-induced effective longitudinal field, which determine the energy efficiency of chiral spin object motion and the stability of the homochiral spin structure, respectively, gradually decrease as the repetition number increases.

ACKNOWLEDGMENTS

This work was supported by the Japan Society for the Promotion of Science (JSPS) KAKENHI (Grants No. 15H05702, No. 26103002, No. 17H05181, No. 17H04924, No. 16H05977, No. 18K19021, and No. 19J11763), the Collaborative Research Program of the Institute for Chemical Research, Kyoto University, and the R & D project for ICT Key Technology of MEXT from the JSPS. This work was partly supported by The Cooperative Research Project Program of the Research Institute of Electrical Communication, Tohoku University. D.-H. Kim was supported as an Overseas Researcher under the Postdoctoral Fellowship of JSPS (Grant No. P16314), by NST Research Fellowship for Young Scientist of the National Research Council of Science & Technology (NST), by the POSCO Science Fellowship of POSCO TJ Park Foundation, by the KIST institutional program (Grant No. 2K02450), and a National Research Council of Science & Technology (NST) grant (Project No. 2N45290). D.-Y.K., Y.-S.N., Y.-K.P., and S.-B.C. were supported by Samsung Electronics Co., Ltd, the Samsung Science & Technology Foundation (SSTF-BA1802-07), and the National Research Foundations of Korea (NRF) funded by the Ministry of Science and ICT (MSIT) (2015M3D1A1070465). D.-H.K., D.-Y.K., Y.-K.P., and B.-C.M. were supported by the KIST institutional program (Grant No. 2E29410) and the National Research Council of Science & Technology (Grant No. CAP-16-01-KIST) funded by the Korea government (MSIT). C.-Y.Y. was supported by the National Research Foundations of Korea (NRF-2015M3D1A1070465).

[1] I. E. Dzialoshinskii, J. Exptl. Theoret. Phys. (U.S.S.R.) **32**, 154 (1957) [Sov. Phys. JETP **5**, 1259 (1957)].
[2] T. Moriya, Phys. Rev. **120**, 91 (1960).
[3] A. Fert, V. Cros, and J. Sampaio, Nat. Nanotechnol. **8**, 152 (2013).
[4] J. Sampaio, V. Cros, S. Rohart, A. Thiaville, and A. Fert, Nat. Nanotechnol. **8**, 839 (2013).
[5] W. Jiang, P. Upadhyaya, W. Zhang, G. Yu, M. B. Jungfleisch, F. Y. Fradin, J. E. Pearson, Y. Tserkovnyak, K. L. Wang, O. Heinonen, S. G. E. te Velthuis, and A. Hoffmann, Science **349**, 283 (2015).
[6] S. Woo, K. Litzius, B. Krüger, M.-Y. Im, L. Caretta, K. Richter, M. Mann, A. Krone, R. M. Reeve, M. Weigand, P. Agrawal, I. Lemesh, M.-A. Mawass, P. Fischer, M. Kläui, and G. S. D. Beach, Nat. Mater. **15**, 501 (2016).
[7] K.-W. Moon, D.-H. Kim, S.-C. Yoo, S.-G. Je, B. S. Chun, W. Kim, B.-C. Min, C. Hwang, and S.-B. Choe, Sci. Rep. **5**, 9166 (2015).
[8] G. Chen, Nat. Phys. **13**, 112 (2017).
[9] W. Jiang, X. Zhang, G. Yu, W. Zhang, X. Wang, M. B. Jungfleisch, J. E. Pearson, X. Cheng, O. Heinonen, K. L. Wang, Y. Zhou, A. Hoffmann, and S. G. E. te Velthuis, Nat. Phys. **13**, 162 (2017).
[10] K. Litzius, I. Lemesh, B. Krüger, P. Bassirian, L. Caretta, K. Richter, F. Büttner, K. Sato, O. A. Tretiakov, J. Förster, R. M. Reeve, M. Weigand, I. Bykova, H. Stoll, G. Schütz, G. S. D. Beach, and M. Kläui, Nat. Phys. **13**, 170 (2017).
[11] S.-G. Je, D.-H. Kim, S.-C. Yoo, B.-C. Min, K.-J. Lee, and S.-B. Choe, Phys. Rev. B **88**, 214401 (2013).
[12] D.-Y. Kim, D.-H. Kim, and S.-B. Choe, Appl. Phys. Express **9**, 053001 (2016).
[13] D.-H. Kim, S.-C. Yoo, D.-Y. Kim, B.-C. Min, and S.-B. Choe, Sci. Rep. **7**, 45498 (2017).
[14] S. Kim, P.-H. Jang, D.-H. Kim, M. Ishibashi, T. Taniguchi, T. Moriyama, K.-J. Kim, K.-J. Lee, and T. Ono, Phys. Rev. B **95**, 220402(R) (2017).
[15] Y. Yoshimura, K.-J. Kim, T. Taniguchi, T. Tono, K. Ueda, R. Hiramatsu, T. Moriyama, K. Yamada, Y. Nakatani, and T. Ono, Nat. Phys. **12**, 157 (2016).
[16] D.-Y. Kim, M.-H. Park, Y.-K. Park, J.-S. Kim, Y.-S. Nam, H.-C. Choi, D.-H. Kim, S.-G. Je, B.-C. Min, and S.-B. Choe, NPG Asia Mater. **10**, e464 (2018).
[17] D.-Y. Kim, M.-H. Park, Y.-K. Park, J.-S. Kim, Y.-S. Nam, H.-S. Hwang, D.-H. Kim, S.-G. Je, B.-C. Min, and S.-B. Choe, Phys. Rev. B **97**, 134407 (2018).
[18] D.-H. Kim, M. Haruta, H.-W. Ko, G. Go, H.-J. Park, T. Nishimura, D.-Y. Kim, T. Okuno, Y. Hirata, Y. Futakawa, H. Yoshikawa, W. Ham, S. Kim, H. Kurata, A. Tsukamoto, Y. Shiota, T. Moriyama, S.-B. Choe, K.-J. Lee, and T. Ono, Nat. Mater. **18**, 685 (2019).
[19] Y.-K. Park, D.-Y. Kim, J.-S. Kim, Y.-S. Nam, M.-H. Park, H.-C. Choi, B.-C. Min, and S.-B. Choe, NPG Asia Materials **10**, 995 (2018).
[20] J. Torrejon, J. Kim, J. Sinha, S. Mitani, M. Hayashi, M. Yamanouchi, and H. Ohno, Nat. Commun. **5**, 4655 (2014).
[21] J. Yu, X. Qiu, Y. Wu, J. Yoon, P. Deorani, J. M. Besbas, A. Manchon, and H. Yang, Sci. Rep. **6**, 32629 (2016).
[22] S. Kim, K. Ueda, G. Go, P.-H. Jang, K.-J. Lee, A. Belabbes, A. Manchon, M. Suzuki, Y. Kotani, T. Nakamura, K. Nakamura, T. Koyama, D. Chiba, K. T. Yamada, D.-H. Kim, T. Moriyama, K.-J. Kim, and T. Ono, Nat. Commun. **9**, 1648 (2018).
[23] I. M. Miron, G. Gaudin, S. Auffret, B. Rodmacq, A. Schuhl, S. Pizzini, J. Vogel, and P. Gambardella, Nat. Mater. **9**, 230 (2010).
[24] I. M. Miron, K. Garello, G. Gaudin, P.-J. Zermatten, M. V. Costache, S. Auffret, S. Bandiera, B. Rodmacq, A. Schuhl, and P. Gambardella, Nature (London) **476**, 189 (2011).
[25] L. Liu, C.-F. Pai, Y. Li, H. W. Tseng, D. C. Ralph, and R. A. Buhrman, Science **336**, 555 (2012).
[26] J. Kim, J. Sinha, M. Hayashi, M. Yamanouchi, S. Fukami, T. Suzuki, S. Mitani, and H. Ohno, Nat. Mater. **12**, 240 (2013).
[27] Y. Fan, P. Upadhyaya, X. Kou, M. Lang, S. Takei, Z. Wang, J. Tang, L. He, L.-T. Chang, M. Montazeri, G. Yu, W. Jiang,

T. Nie, R. N. Schwartz, Y. Tserkovnyak, and K. L. Wang, Nat. Mater. **13**, 699 (2014).

[28] W. S. Ham, S. Kim, D.-H. Kim, K.-J. Kim, T. Okuno, H. Yoshikawa, A. Tsukamoto, T. Moriyama, and T. Ono, Appl. Phys. Lett. **110**, 242405 (2017).

[29] M. DC, R. Grassi, J.-Y. Chen, M. Jamali, D. R. Hickey, D. Zhang, Z. Zhao, H. Li, P. Quarterman, Y. Lv, M. Li, A. Manchon, K. A. Mkhoyan, T. Low, and J.-P. Wang, Nat. Mater. **17**, 800 (2018).

[30] O. Gomonay, T. Jungwirth, and J. Sinova, Phys. Rev. Lett. **117**, 017202 (2016).

[31] T. Shiino, S.-H. Oh, P. M. Haney, S.-W. Lee, G. Go, B.-G. Park, and K.-J. Lee, Phys. Rev. Lett. **117**, 087203 (2016).

[32] K.-J. Kim, S. K. Kim, Y. Hirata, S.-H. Oh, T. Tono, D.-H. Kim, T. Okuno, W. S. Ham, S. Kim, G. Go, Y. Tserkovnyak, A. Tsukamoto, T. Moriyama, K.-J. Lee, and T. Ono, Nat. Mater. **16**, 1187 (2017).

[33] C. Moreau-Luchaire, C. Moutafis, N. Reyren, J. Sampaio, C. A. F. Vaz, N. V. Horne, K. Bouzehouane, K. Garcia, C. Deranlot, P. Warnicke, P. Wohlhüter, J.-M. George, M. Weigand, J. Raabe, V. Cros, and A. Fert, Nat. Nanotechnol. **11**, 444 (2016).

[34] E. N. Abarra, B. R. Acharya, A. Inomata, and I. Okamoto, Fujitsu Sci. Tech. J. **37**, 145 (2001).

[35] A. V. Davydenko, A. G. Kozlov, A. G. Kolesnikov, M. E. Stebliy, G. S. Suslin, Yu. E. Vekovshinin, A. V. Sadovnikov, and S. A. Nikitov, Phys. Rev. B **99**, 014433 (2019).

[36] K.-S. Lee, D.-H. Kim, and S.-B. Choe, J. Magn. **15**, 99 (2010).

[37] S.-G. Je, S.-C. Yoo, J.-S. Kim, Y.-K. Park, M.-H. Park, J. Moon, B.-C. Min, and S.-B. Choe, Phys. Rev. Lett. **118**, 167205 (2017).

[38] P. P. J. Haazen, E. Murè, J. H. Franken, R. Lavrijsen, H. J. M. Swagten, and B. Koopmans, Nat. Mater. **12**, 299 (2013).

[39] D.-Y. Kim, N.-H. Kim, Y.-K. Park, M.H. Park, J.-S. Kim, Y.-S. Nam, J. Jung, J. Cho, D.-H. Kim, J.-S. Kim, B.-C. Min, S.-B. Choe, and C.-Y. You, Phys. Rev. B **100**, 224419 (2019).

[40] S. Bandiera, R. C. Sousa, B. Rodmacq, and B. Dieny, IEEE Magn. Lett. **2**, 3000504 (2011).

[41] D.-H. Kim, S.-C. Yoo, D.-Y Kim, K.-W. Moon, S.-G Je, C.-G. Cho, B.-C. Min, and S.-B. Choe, Appl. Phys. Lett. **104**, 142410 (2014).

[42] T. Nishimura, M. Haruta, D.-H. Kim, Y. Shiota, H. Iwaki, D. Kan, T. Moriyama, H. Kurata, and T. Ono, J. Magn. Soc. Jpn. **44**, 9 (2020).